UCRL 2387

UNCLASSIFIED

UNIVERSITY OF CALIFORNIA

Radiation Laboratory

BERKELEY, CALIFORNIA

DISCLAIMER

This document was prepared as an account of work sponsored by the United States Government. While this document is believed to contain correct information, neither the United States Government nor any agency thereof, nor the Regents of the University of California, nor any of their employees, makes any warranty, express or implied, or assumes any legal responsibility for the accuracy, completeness, or usefulness of any information, apparatus, product, or process disclosed, or represents that its use would not infringe privately owned rights. Reference herein to any specific commercial product, process, or service by its trade name, trademark, manufacturer, or otherwise, does not necessarily constitute or imply its endorsement, recommendation, or favoring by the United States Government or any agency thereof, or the Regents of the University of California. The views and opinions of authors expressed herein do not necessarily state or reflect those of the United States Government or any agency thereof or the Regents of the University of California.

UCRL-2337
Unclassified - Physics Distribution

UNIVERSITY OF CALIFORNIA

Radiation Laboratory

Contract No. W-7405-eng-48

THE VARIATION OF HIGH-ENERGY TOTAL NEUTRON CROSS SECTIONS WITH ENERGY

Boris Ragent
(Thesis)

August 28, 1953

Berkeley, California

THE VARIATION OF HIGH-ENERGY TOTAL NEUTRON CROSS SECTIONS WITH ENERGY

TABLE OF CONTENTS

Abstract 3

Introduction 4

Experimental Method 7

Time-of-Flight Technique

Total Cross Section Measurements

Alignment, Background, Sources of Error

Results 24

Treatment of Data

Calculation of Cross Sections

Discussion of Results 40

Acknowledgments

References

THE VARIATION OF HIGH-ENERGY TOTAL NEUTRON CROSS SECTIONS WITH ENERGY

Boris Ragent

Radiation Laboratory, Department of Physics
University of California, Berkeley, California

August 28, 1953

ABSTRACT

The total neutron cross sections for carbon, iron, antimony, and tantalum have been measured in the region of 35 to 180 Mev in a good geometry absorption experiment using time-of-flight instrumentation developed for the 184" cyclotron. Tantalum exhibits a shallow dip in the cross section curve in the region of 50 to 70 Mev. It is apparent within the statistics that antimony has a dip in this region, and that iron and carbon also show unexpected behavior at these energies.

THE VARIATION OF HIGH-ENERGY TOTAL NEUTRON CROSS SECTIONS WITH ENERGY

Boris Ragent

Radiation Laboratory, Department of Physics
University of California, Berkeley, California

August 28, 1953

INTRODUCTION

The development of high-energy sources of neutrons within the past decade has given to investigators an extremely useful tool for the investigation of the nucleus and of nuclear properties. The very nature of the high-energy neutron--that is, its absence of electric charge and its short wave length--make it an ideal probing mechanism. However, we have not yet extensively realized the simplification in understanding the nucleus which we had hoped to gain from the results of measurements on nuclei bombarded with high-energy particles. The measurements on total cross sections for neutrons, which yield interesting information on the nuclear radius and--it is thought--on the nuclear potentials, have not yielded results as definitive as could be hoped. Even the recent information at low neutron energies, in the one- to three-Mev energy region, has yielded data inconsistent with the prior notions of what constituted the mean free path for nucleons in the nucleus.[1] An attempt to explain these phenomena at low energies has been made by Weisskopf[2], who finds remarkable agreement with experimental values by assuming a very small absorption coefficient for nuclei--that is, a long mean free path, or alternatively, a small sticking probability.

At somewhat higher neutron energies, of the order of 14 Mev, the nucleus has been considered as an opaque spherical diffracting object that would yield cross sections of $2\pi R^2$, R being the nuclear radius. Several investigators have been measurements in this region that agreed fairly well with this concept.

At even higher neutron energies the wave length of the neutron becomes of the order of, or smaller than, the nuclear dimensions, and the nucleus should begin to exhibit the so-called "transparency" effects.[3] On this basis Fernbach, Serber, and Taylor constructed the optical model of the nucleus that characterized nuclei by an absorption coefficient and an index of refraction, as well as a radius.[4] The results of the calculations with the optical model agreed fairly satisfactorily with experimental results from the region of about 80 Mev to 300 Mev, using reasonable values for the parameters, and judicious guesses as to the variation of these parameters with energy. However, in order to obtain agreement at 300 Mev, the index of refraction had to be reduced to zero. In particular, this model gave good agreement with the angular distributions of elastically-scattered particles. This was not true until recently, when an exact calculation based on the optical model was carried out.[17]

Measurememts of neutron cross sections at extremely high energies are not likely to yield much direct information on the gross nuclear properties or structure since, at these energies, the interactions are presumably between neutron and nucleon within the nucleus. However, the synthesis of nuclear properties from nucleon-nucleon

interactions will very probably arise from the study of these very high energy phenomena.

The most promising regions in which to investigate the nucleus with the neutron probe, therefore, seems to be the region from about 35 to 180 Mev, since it is just at these wave lengths that the neutron is of an appropriate size. In the past, one of the difficulties in working in this region has been the lack of monoenergetic neutron sources, as well as energy-insensitive detectors. The net effect of such a difficulty has been to make the measurements yield mean values which were weighted over the energy spectrum of the neutron source and the detection efficiency of the detector.[5,6,7] Such measurements, therefore, tended to de-emphasize any fine structure in the total cross-section measurements.

Recently measurements have been made in which it was attempted to narrow the band of energies detected and thus to obtain total cross-section curves as a function of energy.[8,9,10] These experiments, surprisingly, displayed a rather sharp dip in the cross-section curves for lead in the region of approximately 60 Mev, as well as hints of dips in elements of lower atomic number at lower energies.

With the advent of high-speed scintillator detectors and electronic techniques it became feasible to devise a time-of-flight apparatus for high-energy neutrons, and thus desirable to investigate the behavior of the neutron cross section for representative nuclei as a function of energy. The first test of this apparatus was in measuring the total cross section for lead from 35 to 160 Mev and in confirming that a dip actually does occur.[11,12] This report is an extension of the work to other elements.

EXPERIMENTAL METHOD

Time-of-Flight Technique

The neutron time-of-flight technique developed for use with the 184-inch synchro-cyclotron is discussed here only briefly since a comprehensive discussion of the method and apparatus has been made elsewhere.[10,11]

A short burst of high-energy neutrons is obtained by electrostatically deflecting the 190-Mev deuteron beam radially within the tank of the cyclotron until it impinges upon an electrically insulated probe situated two to three inches outside of the equilibrium orbit. This probe is long enough in the direction of the beam to stop the deuterons by ionization loss, and is thin enough radially so that a single rf pulse of the deuterons may be selected from the region outside of the equilibrium orbit. The details of the probe as shown in Figs. 1 and 2. The electrical pulse resulting from the deuterons impinging on the probe is amplified by wide-band amplifiers and is displayed on one of the vertical deflection plates of a high-speed oscilloscope.

Some of the deuterons incident upon the probe are sheared into a proton and neutron each by the so-called "stripping" process,[13] the neutrons proceeding into a small forward cone tangent to the direction of the incident deuteron beam. The protons formed are deflected by the magnetic field out of the forward direction, so that a relatively "clean" beam of high-energy neutrons is obtained in the forward direction. This beam is collimated by approximately two meters of copper, lead, and concrete to a dimension of approximately six inches by six inches at the detector. This results in a collimated beam of neutrons of bunching time

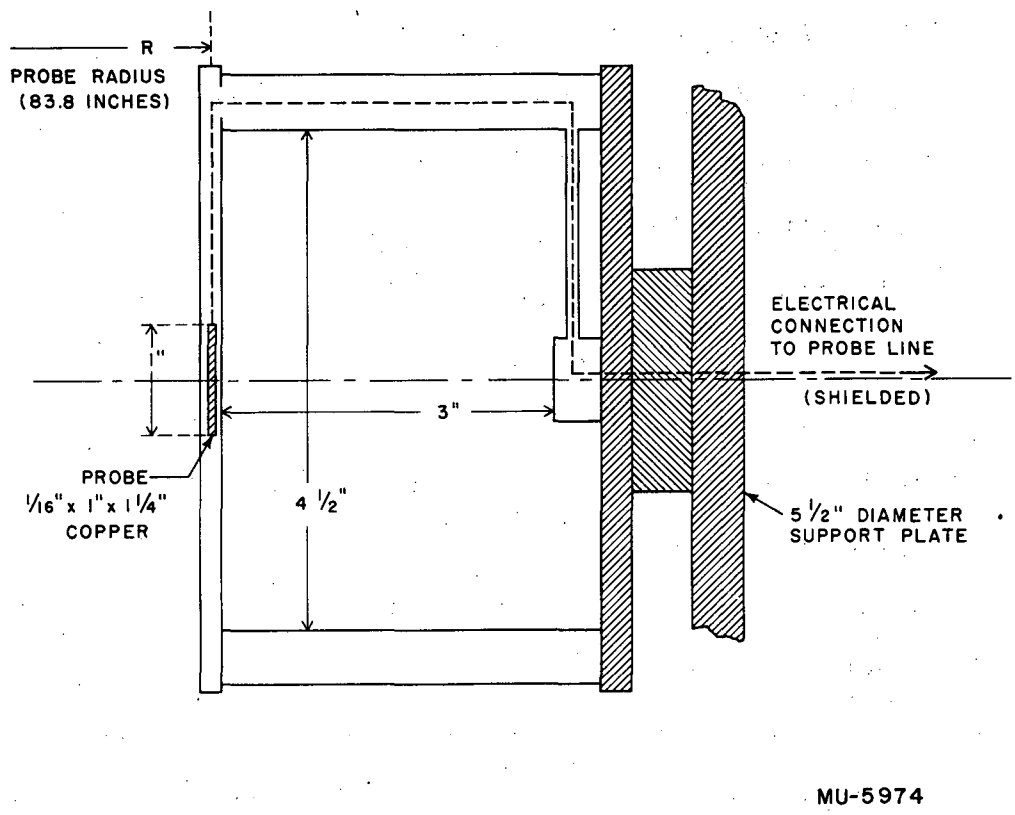

Fig. 1 - Schematic Drawing of Probe Assembly.

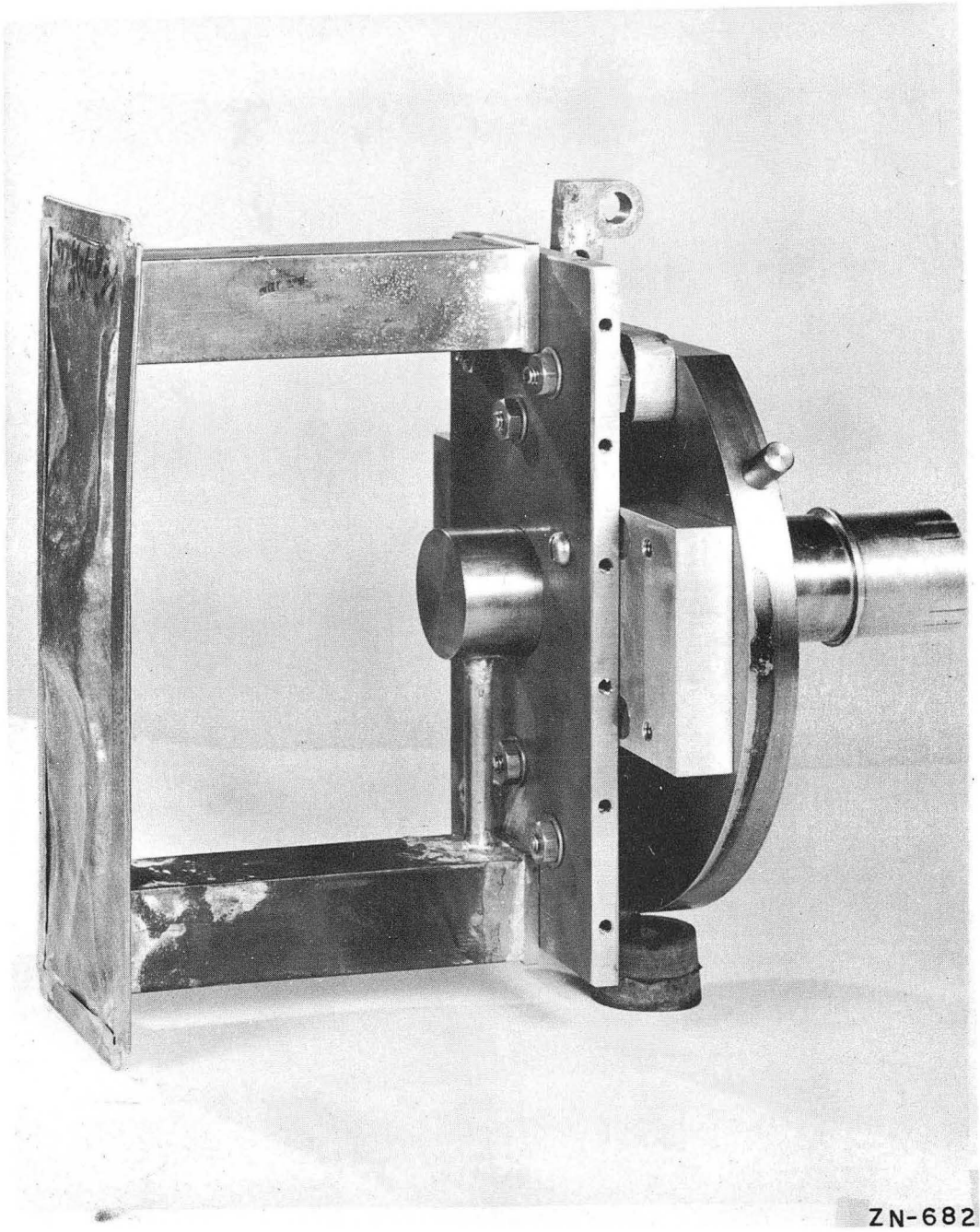

Fig. 2 - Probe Assembly

approximately equal to 7×10^{-9} seconds full-width at half-maximum at the probe and containing a spectrum of energies extending from about 30 to 190 Mev with a peak at approximately 95 Mev.

A detector consisting of a small transstilbene crystal viewed by two 1P21 photomultiplier tubes is placed at the maximum convenient distance (43.7 meters) from the probe on the beam axis. The arrangement is shown in Fig. 3. Pulses from the phototubes arising from proton recoils in the stilbene crystal activate a coincidence circuit whose output is amplified and triggers the sweep on the high-speed oscilloscope. Simultaneously the output of one of the phototubes is amplified and is displayed on the remaining vertical deflection plate of the oscilloscope in a polarity opposed to that of the probe pulse. The time of flight of a neutron (within the uncertainty of the bunching time) is then determined by the distance on the oscilloscope sweep in time between the beginning of the signal pulse and the probe pulse. Calibration of the oscilloscope sweep is accomplished by use of a standard 50-megacycle oscillator. A curve of neutron time of flight versus energy is given in Fig. 4.

The phototubes in the detector are operated at a sensitivity high enough to also detect Compton electrons from γ-rays originating in the probe. By inserting appropriate cable delays, then, in the signal, probe, and trigger lines to the oscilloscope one may obtain a display that contains signal pulses due both to neutrons and to γ-rays, and also the probe pulse. This then automatically calibrates all the delays in the circuit as well as yielding the over all resolution of the entire system, since the γ-rays furnish pulses for a particle of known velocity over a known flight path. By measuring the

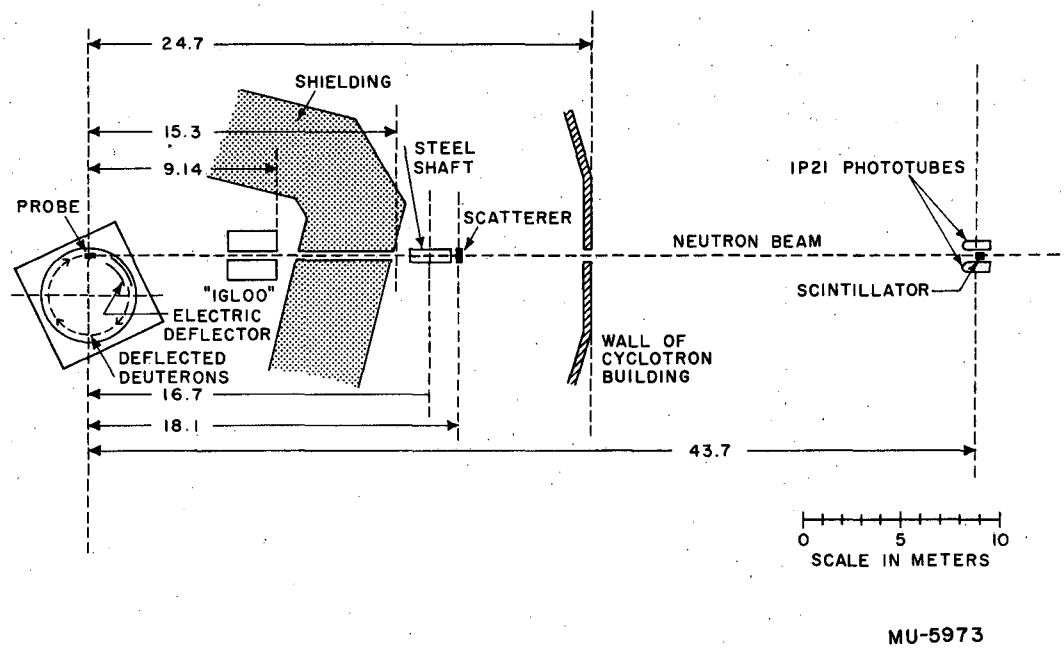

Fig. 3 - Physical Arrangement

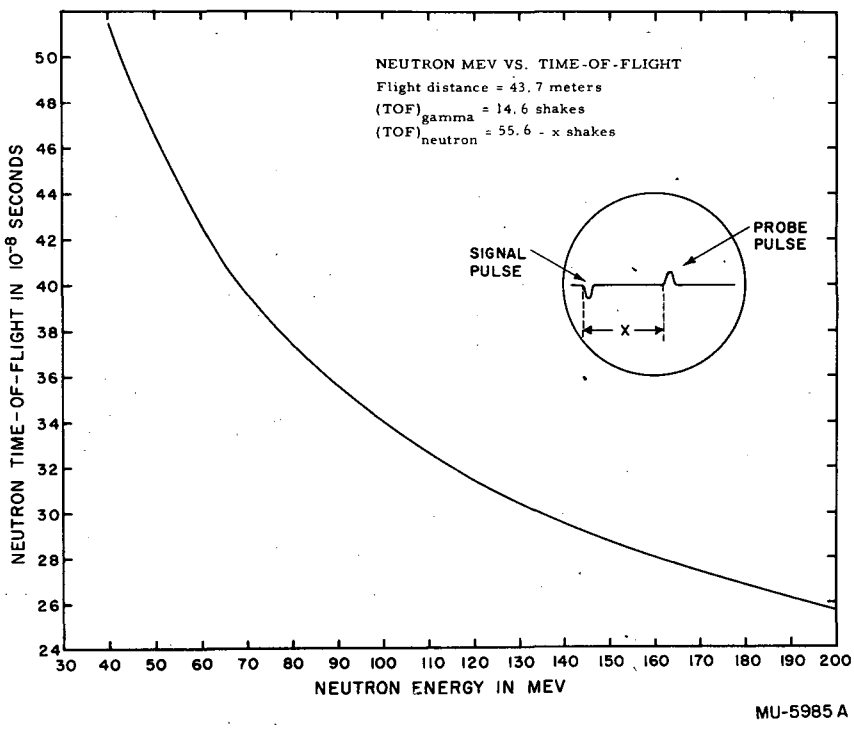

Fig. 4 - Neutron Energy vs. Time of Flight

distribution in time of the γ-rays all the factors entering into the resolution of the system are automatically taken into account. The block diagram of the electronics is shown in Fig. 5 and a typical sweep is shown in Fig. 6.

The counting rate in the detector is adjusted in order to avoid a "jamming" phenomenon by varying the size of the transstilbene crystal. This need for a jamming correction arises from the possibility of having two neutrons activate the detector within such a short period of time that the detector would register only one pulse. For reasonable counting rates this correction can be made negligible.

The oscilloscope is photographed on a continuous-film camera with no shutter, and after development the film is projected onto a calibrated mat, which may be divided into any number of convenient channels for reading purposes.

The ultimate resolution in the system as finally developed for a roughly gaussian γ-ray distribution of 7×10^{-9} seconds full-width at half-maximum and a flight path of 43.7 meters was $\pm 8 \times 10^{-5}$ microseconds/meter.

Total Cross-Section Measurements

The total cross sections for antimony, tantalum, iron, and carbon were measured with the usual good geometry absorption technique. The absorbers in the order listed were interposed into the direct beam of neutrons, and the counts were recorded as previously described with each absorber in place, and with no absorber in place.[10] The number

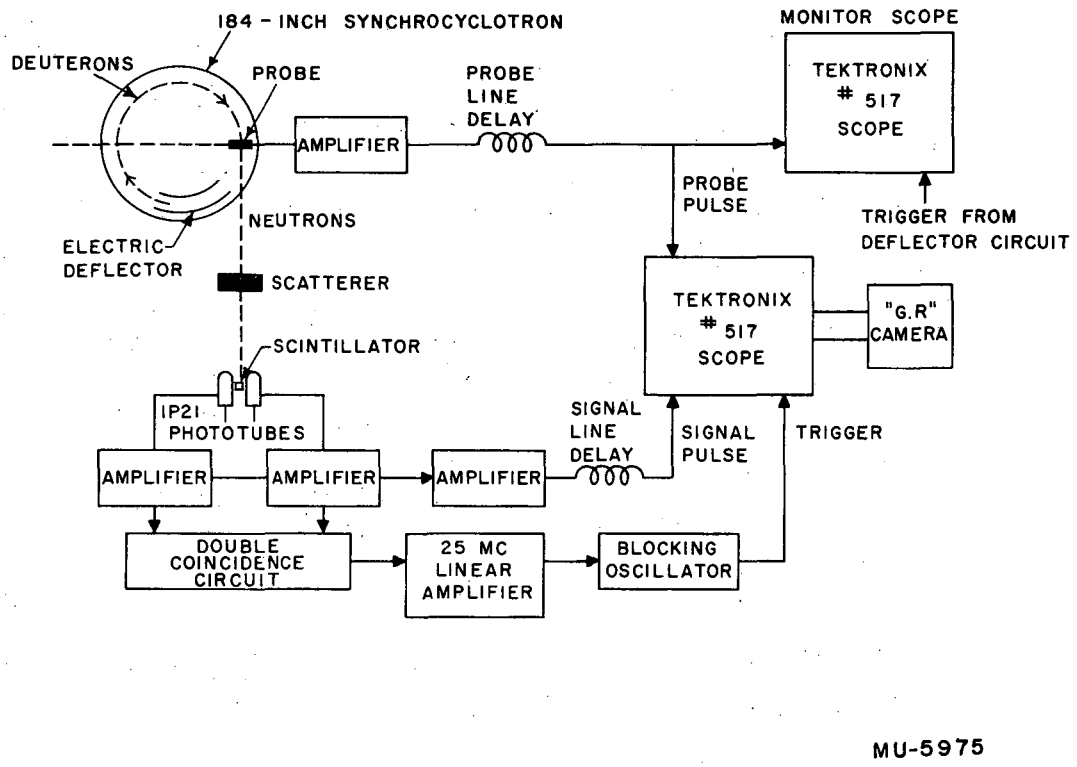

Fig. 5 - Block Diagram of Electronics

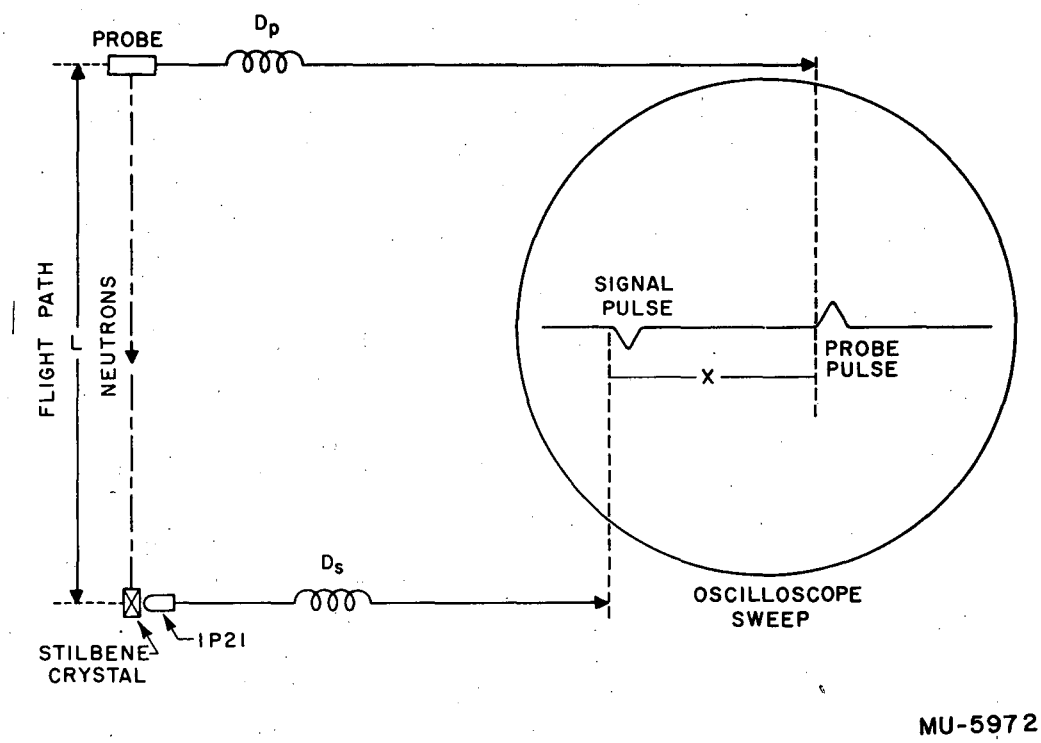

Fig. 6 - Typical Sweep

of counts so recorded was tallied per unit time of flight and the transmission so measured was converted to a relative[10] cross section (since no beam monitor was used) from the equation:

$$\sigma = \frac{1}{N} \ln\left(\frac{1}{T}\right) \quad , \quad \Delta\sigma = \frac{1}{N}\left[\frac{1}{I_o} + \frac{1}{I}\right]^{\frac{1}{2}} \qquad (1)$$

where $T = \dfrac{I - B_I}{I_o - B_{I_o}}$ is the transmission, N is the number of nuclei per cm^2 in the path of the beam, I_o is the number of counts without absorber, I is the number of counts with absorber, and B_{I_o} and B_I are the respective backgrounds. As will be described later, B_{I_o} and B_I were negligibly small.

The reason that the cross section was measured on a relative basis was twofold. First, the main interest in these measurements has been to investigate the variation with energy of the cross sections, and since each burst of neutrons contains a complete spectrum of energies it is only the comparison between the spectra with and without absorber that is necessary for our purpose. Second, in order to measure an absolute cross section, a beam monitor would have had to be employed. This would have had to be of an electronic type in order to avoid counting any background neutrons not due to the main burst, and thus would suffer from the same jamming phenomenon previously discussed. If the counting rate were adjusted in the monitor to avoid jamming, the total cyclotron running time in order to achieve the statistical accuracy desired would have had to be increased by a factor of about four.

Furthermore, since the cross section of carbon had been measured over an overlapping energy region by at least three different observers,[9,10,14]

the cross-section curves could be normalized on an absolute basis at a point of agreement by referring all such curves to carbon at that point from the relation

$$\sigma_x = \frac{N_{carbon}}{N_x} \sigma_{carbon} = \frac{1}{N_x} \ln \frac{I_x}{I_{carbon}} \qquad (2)$$

from which the error (from the law of the propagation of errors) is

$$\Delta \sigma_x = \frac{1}{N_x} \left[(N_{carbon} \quad \Delta \sigma_{carbon})^2 + \frac{1}{I_{carbon}} + \frac{1}{I_x} \right]^{\frac{1}{2}} \qquad (2a)$$

The point chosen for normalization was one at which the cross section for carbon was not varying rapidly with energy, and at which the statistical accuracy of I_c and I_x were good.

In making the measurements the absorbers, which were mounted on a cart perpendicular to the beam axis about 18 meters from the probe, were changed at three- minute intervals without turning off the beam. The thicknesses of absorbers were adjusted so as to give almost equal counting rates.

The absorbers were accurately machined blocks, except for tantalum, in which case the material consisted of smooth sheets of metal varying in thickness from one-eighth of an inch to one-thirty-second of an inch mounted in a special holder which held the sheets under compression. In all cases the dimensions perpendicular to the beam were larger than the beam. The actual values of the absorber dimensions are given in Table I, and the arrangement of the apparatus is shown in Figs. 3 and 7.

ABSORBER DIMENSIONS

Absorber		Dimensions	χ Toward beam	Mass	Density	Atomic Wt.	N = No. of Atoms per sq. Cm.	$\frac{1}{N}$
TANTALUM		4.020"x8.025"x4.673"	11.85cms	39,984gms	16.19	180.88	6.395×10^{23}	1.562×10^{-24}
ANTIMONY	I	3.374"x5.880"x5.872"	25.59cms	12,749	6.685	121.76	8.453×10^{23}	1.182×10^{-24}
	II	3.206"x5.891"x5.851"		12,089				
	III	3.490"x5.993"x6.092"						
IRON	I	1.487"x3.983"x8.116"	15.06cms	6,117.0	7.853	55.85	12.79×10^{23}	$.784 \times 10^{-24}$
	II	1.480"x3.973"x8.113"		6,133.8				
	III	1.487"x3.986"x8.109"		6,180.5				
	IV	1.483"x3.972"x8.109"		6,145.1				
	V	1.481"x3.945"x8.204"		6,174.1				
	VI	1.481"x3.945"x8.204"		6,176.7				
	VII	1.481"x3.945"x8.204"		6,175.9				
	VIII	1.481"x3.945"x8.203"		6,177.0				
CARBON	I	9.000"x6.000"x6.000"	68.57	8,864	1.693	12.01	5.83×10^{24}	$.1716 \times 10^{-24}$
	II	8.995"x6.000"x6.000"		8,797				
	III	9.000"x5.996"x5.995"		9,288				

TABLE I

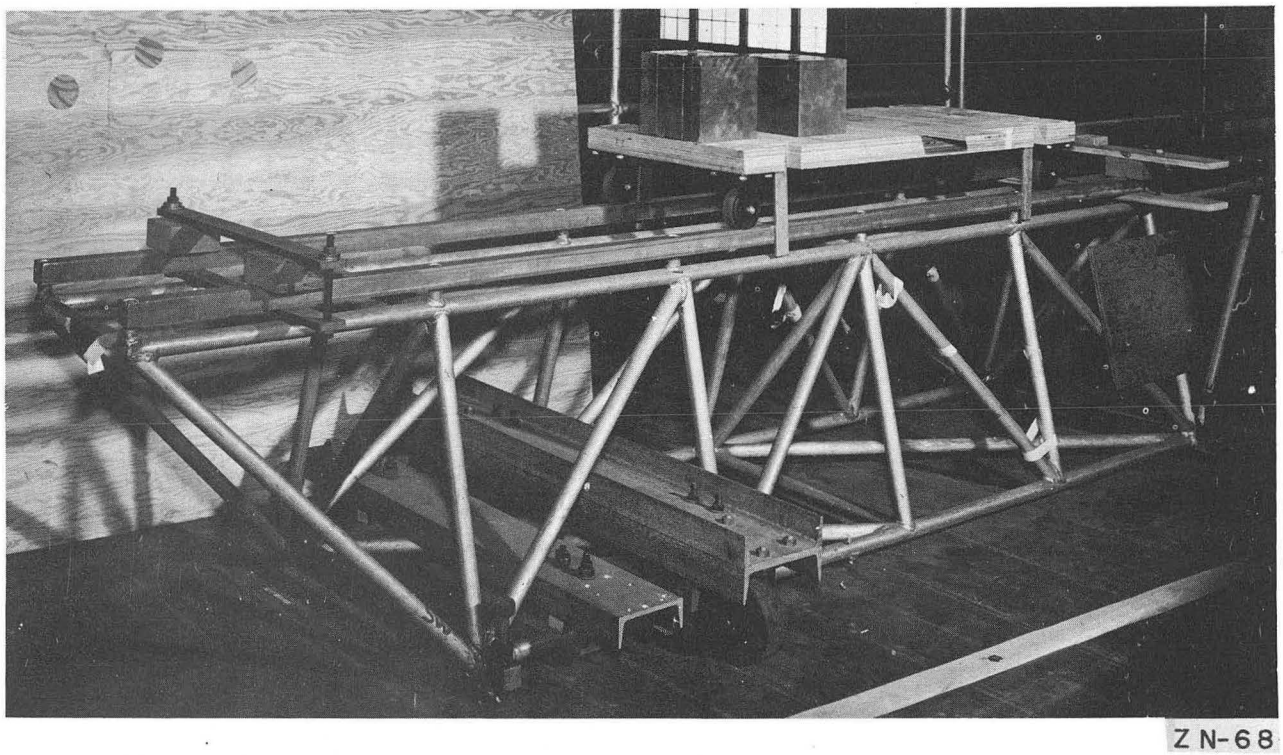

Fig. 7 - Scattering Bench.

UCRL-9337

Alignment, Background, Sources of Error

1. Alignment

Initial alignment over the 43.7-meter path was accomplished with a cathetometer. The beam at the detector was also mapped by moving the detector and recording the counting rates. The width of the beam so mapped was almost exactly six inches, and fell off rather steeply when the detector was moved more than three inches in a vertical or horizontal direction off the beam axis. A check on the absorber alignment was made by plotting the counting rate of the detector as a function of absorber traverse. Finally a traverse perpendicular to the beam was made with a bar of iron three inches in diameter by six feet long. All these measurements insured that the equipment was aligned to within one-eighth inch over the entire flight path. Since the minimum overlap of the absorbers was one-half inch and the detector was only 0.5cm x 1.0 cm x 1.5 cm it was felt that the alignment was satisfactory.

2. Background

There are three types of background counts to be considered.

The first is caused when more than one rf pulse of deuterons strikes the probe. This might necessitate a "recycling" correction, to use the terminology of low-energy time-of-flight workers. The separation in time of the deuteron pulses would be about 10^{-7} seconds, the period of the rf of the cyclotron. The recycling would give rise to counts beyond the maximum cutoff energy of the cyclotron as calculated on a time-of-flight basis.

Precautions were taken to prevent recycling by monitoring the probe pulse (so as to note the appearance of any secondary pulse), as described

in Reference 10, and by analyzing the film to detect such counts, several times during the run. In all, the recycling or spurious counts amounted to about 10 counts out of approximately 65,000 data counts. It is, therefore thought that this correction is negligible.

The second type of background is that due to random counts in the detector caused by cosmic rays, noise pulses, and activation of the carbon in the transstilbene by the $C^{12}(n, 2n)C^{11}$ reaction. This background is in general of a random nature, and is not connected with the beam pulse except for that associated with the carbon activation. It is characterized on the oscilloscope by the presence of a sweep and signal pulse without a probe pulse. This appearance also happens to be characteristic of low-energy neutron events, for which the probe pulse is too far to the left of the sweep to be read. In any event these "blank" sweeps are discarded. The chance that a coincidence will occur between a probe pulse and a random count during a beam pulse is too small to be considered.

The third type of background, and the most difficult to assess, is that due to particles scattered into the detector from neutrons, in particular particles scattered from the walls of the building, supports, and other objects, and from the long air path. An attempt to estimate the contribution due to this effect was made by inserting a steel shaft three inches in diameter by six feet long in place of the absorbers. This insured that almost all the incident neutrons would be scattered out of the beam, hence would perhaps accentuate the effect. Also, the shaft was slightly smaller than the beam dimensions, so that some small-angle elastic scattering could have occurred. The effect of introducing the shaft was to lower

the counting rate of the detector to much less than one percent of its counting rate with no absorber, and in fact was statistically insignificant. This measurement along with the large distances involved and the small solid angle presented by the detector for any scattering process gave confidence that this background was also very small.

3. Sources of Error

a. Diffraction Scattering

Generally two to three mean free paths of absorber were used, except for carbon where the number of mean free paths varied from two to six over the energy region covered. By the method of DeJuren[15] or of McMillan and Sewell,[16] the maximum correction to the data was found to be of the order of one-tenth of one percent; it was accordingly not made.

b. Systematic Errors

Systematic errors are by their very nature unknown, since if they were known they would be corrected. The most serious systematic error that could occur in this experiment would be a transient change in the time-of-flight calibration of the system. In particular this change would cause an apparent shift in the energy spectrum of neutrons with absorber, and that without absorber. This shift would lead to spurious dips in the cross-section curve that could not be divorced from any real effects, which would show up similarly. It is hoped, of course, that no such change did occur, and in fact each reel of film taken with absorbers in place had at least a few γ-ray pulses at the appropriate mean of the previously measured γ-ray spectrum. Unfortunately there

were not enough γ-rays present getting through the absorbers to make the constancy of the calibration a statistical certainty. On the other hand, it is difficult to imagine any process that would change the energy calibration in a manner that would not have been detected.

A second type of systematic error may be a human one, that is, the tendency of an observer to read data more favorably into certain channels than others, especially in borderline cases. Certain control checks were attempted in this regard, but here again it can only be hoped that the author, who did all the film reading, either was consistently off in his readings of I_o and I or was sufficiently unbiased.

RESULTS

Treatment of Data

1. Energy Calibration and Resolution

The film, after processing, was projected onto the screen of a microfilm projector. Using the 50-megacycle traces, present on each reel, a mat was constructed having lines at 10^{-8}-second intervals. The distribution of γ-rays was next plotted on a more exact basis, tabulating these pulses into 2×10^{-9}-second channels. This distribution was roughly gaussian in shape and comprised 172 samples yielding a full-width at half-maximum of 0.7×10^{-8} seconds. From the position of the mean of this distribution and the known flight time for γ-rays of 14.58×10^{-8} seconds, each line on the mat was calibrated on a relativistic basis. The mean energy corresponding to the center of each 10^{-8}-second interval was then computed.

The data were treated on an individual channel basis corresponding to the means determined above, and also on a grouped basis in order to improve the statistics. In order to calculate the mean energy of a group of channels the channels were weighted according to the I_o spectrum such that

$$E_{mean} = \frac{\sum N_J E_J}{\sum N_J}, \quad \text{or actually on a time basis}$$

corresponding to

$$T_{mean} = \frac{\sum N_J T_J}{\sum N_J}$$

The energy resolution is usually arbitrarily defined. In this case one-fourth of each channel width (the probable error of a channel) was combined by propagation of errors with the probable error due to the neutron bunching time (corresponding to approximately 2×10^{-9} seconds), the result being divided by 0.6745 to yield the standard deviation in energy, ΔE. The uncertainty in energy was then calculated from the relativistic formula $\Delta E = \frac{\Delta E}{\Delta t} \Delta t$, $\beta = \frac{v}{c} = \frac{\text{velocity of neutron}}{\text{velocity of light}}$

where

$$\frac{\Delta E}{\Delta t} = -(\beta\gamma)^2 \gamma \frac{M_0 c^2}{t}$$

$M_0 c^2$ = rest energy of neutron = 939.43 Mev

t = time of flight of neutron

$$\gamma = \frac{1}{\sqrt{1-\beta^2}}$$

2. Normalization of Data

The data which were calcuated on an individual channel basis were normalized at 100 Mev using the results of three observers.[9,10,14] The value used at this point was $\sigma_{\text{Total carbon}} = 475 \pm 10$ millibarns.

For the grouped data a point on the carbon cross section was chosen at 102.8 Mev, at which point the carbon cross section was taken as $\sigma_t = 462 \pm 6$ mb.

The cross sections and the associated errors at the normalization points were calculated from formula (2). Since this is a valid method for determining cross sections and since in general the statistical error associated with this method of calculation was greater than or approximately equal to the statistical error associated with the direct-beam comparison method, the errors quoted were those from the direct-beam comparison method. This was done because the estimates on the

errors of the normalization point were extremely generous. In any event, this normalization error affects the entire cross-section curve equally and may be considered as an error on the absolute scale of the cross section rather than on the individual points themselves. (In other words, the entire curve goes up or down according to the normalization error, rather than any one point.)

Calculation of Cross Section

The individual channel cross sections and their standard deviations wer calculated using formula (1). For some of these data it can be seen that the statistical errors are quite large. Therefore, the data were recalculated for each element, grouping channels together, to achieve the maximum statistical accuracy still consistent with a reasonable energy resolution. The groupings varied from five channels at the low-energy end to two channels. The individual channel data are tabulated in Table II and plotted in Figs. 8 - 11, while the grouped data are given in Table III and Fig. 12.

For comparison purposes, the plots of the spectra of the direct beam and the elements on a time-of-flight basis, and the direct beam as a function of energy, corrected for the n - p cross section,[19] are given in Figs. 13 to 18.

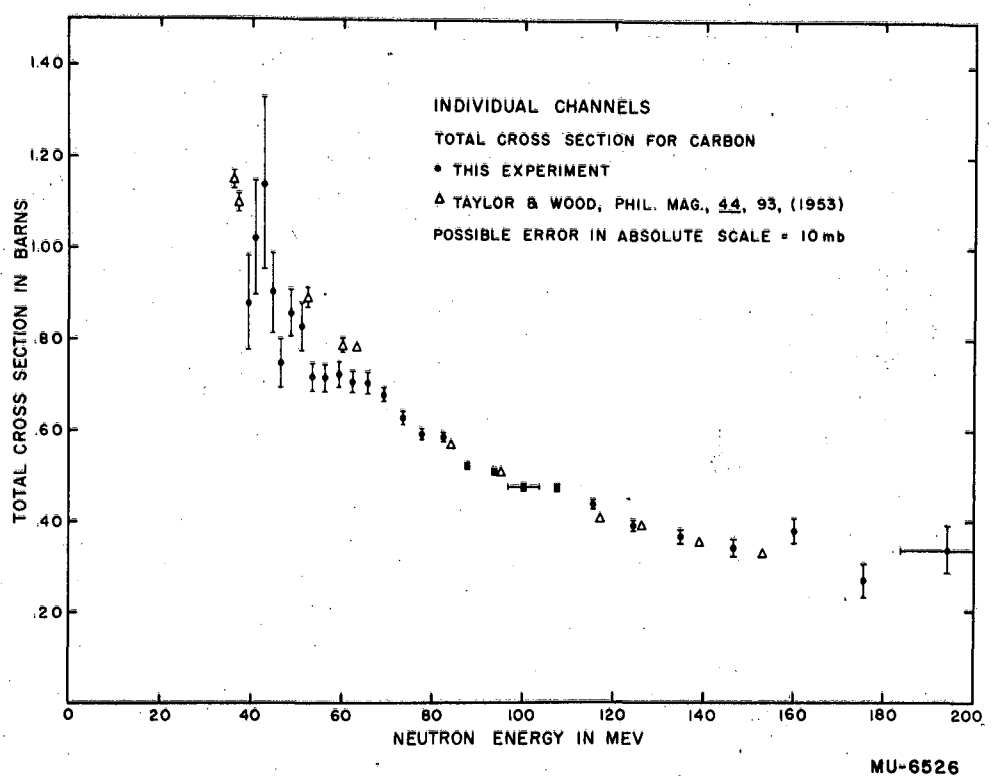

Fig. 8 - Individual Channels, Total Cross section for Carbon

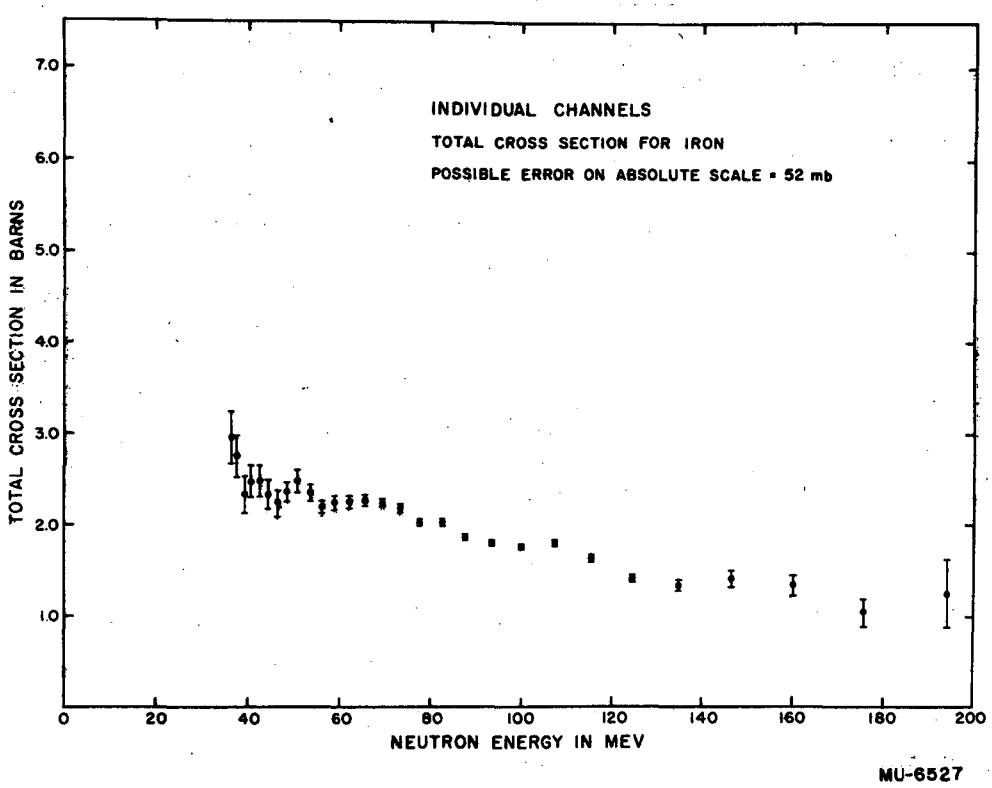

Fig. 9 - Individual Channels, Total Cross Section of Iron

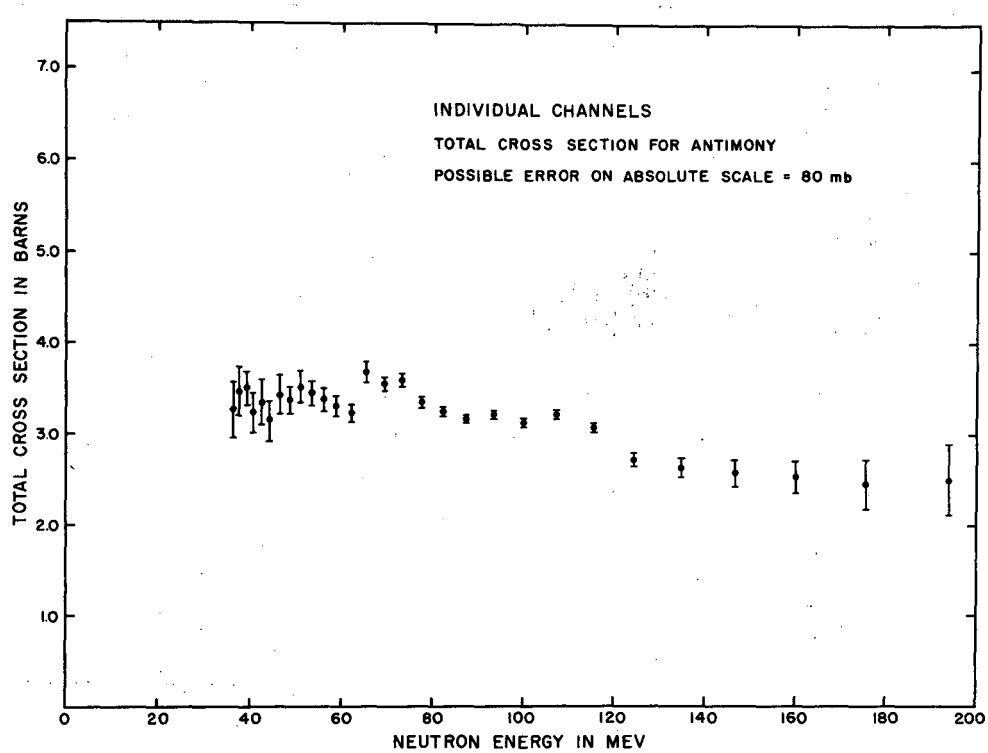

Fig. 10 - Individual Channels, Total Cross Section for Antimony

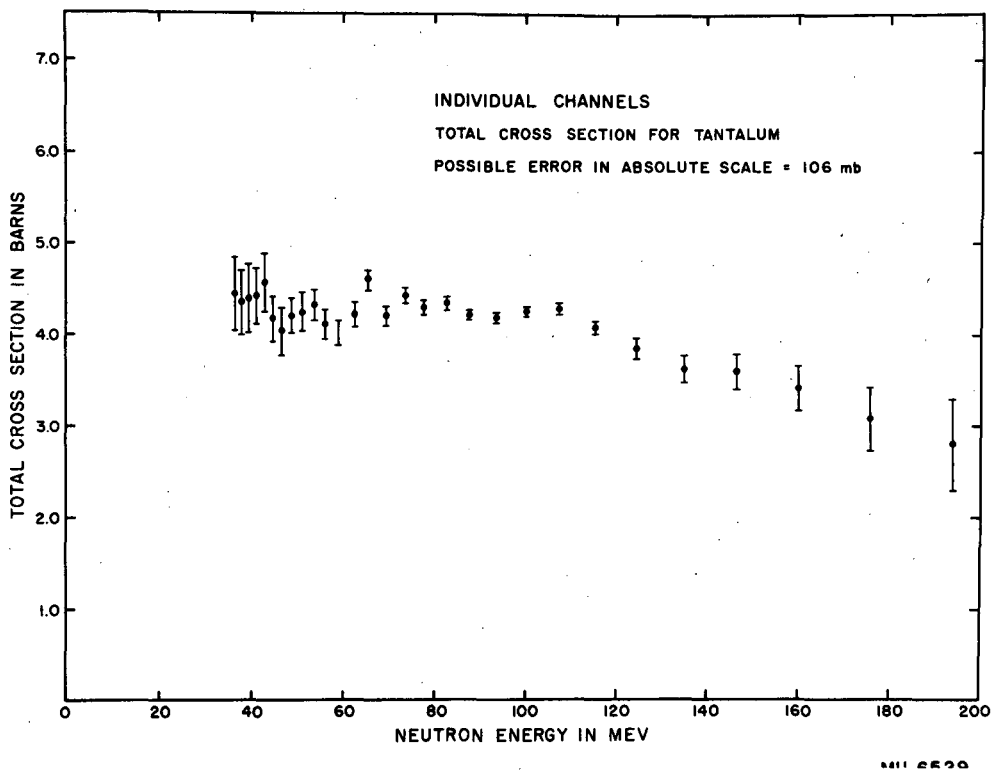

Fig. 11 - Individual Channels, Total Cross section for Tantalum

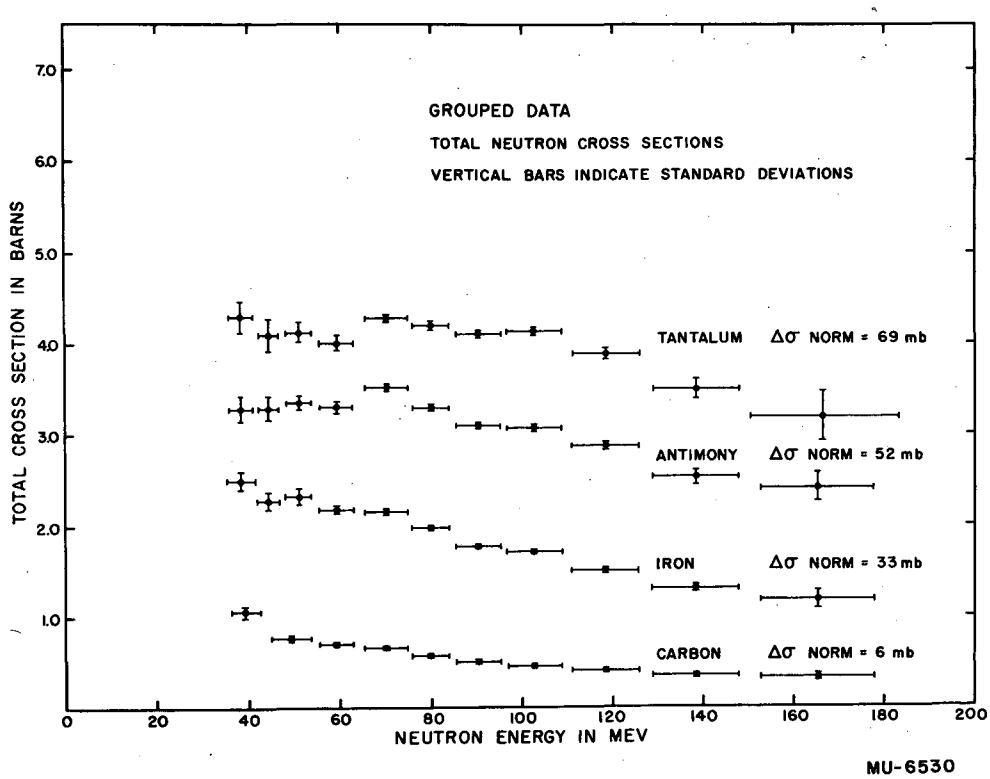

Fig. 12 - Grouped Data, Total Neutron Cross Section

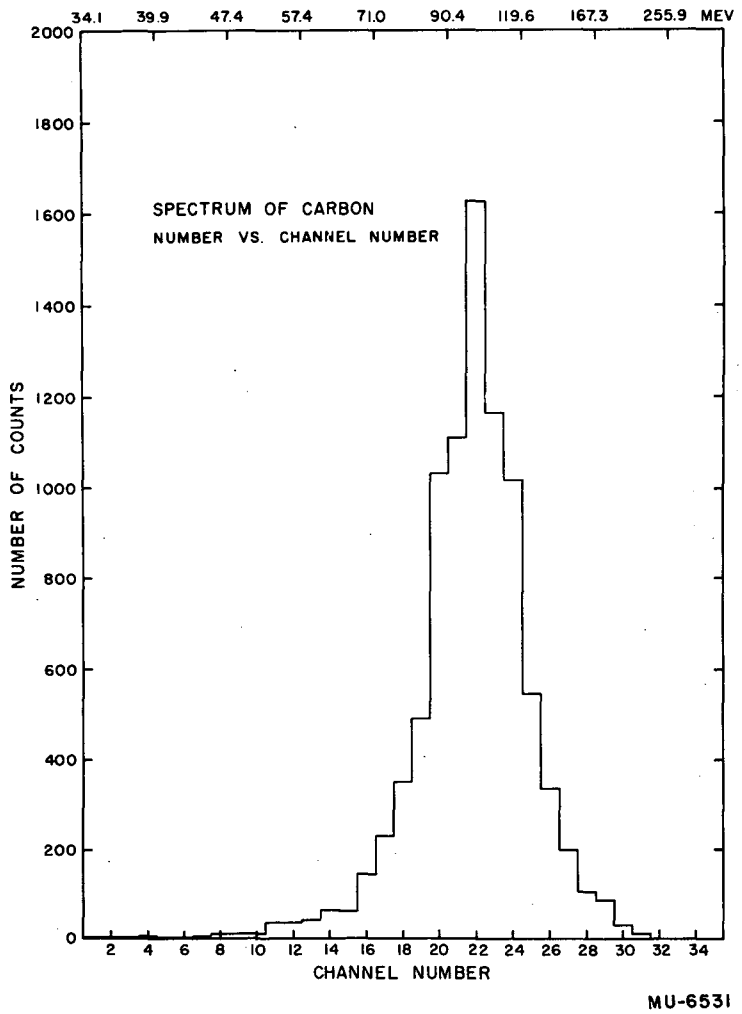

Fig. 13 - Spectrum of Carbon

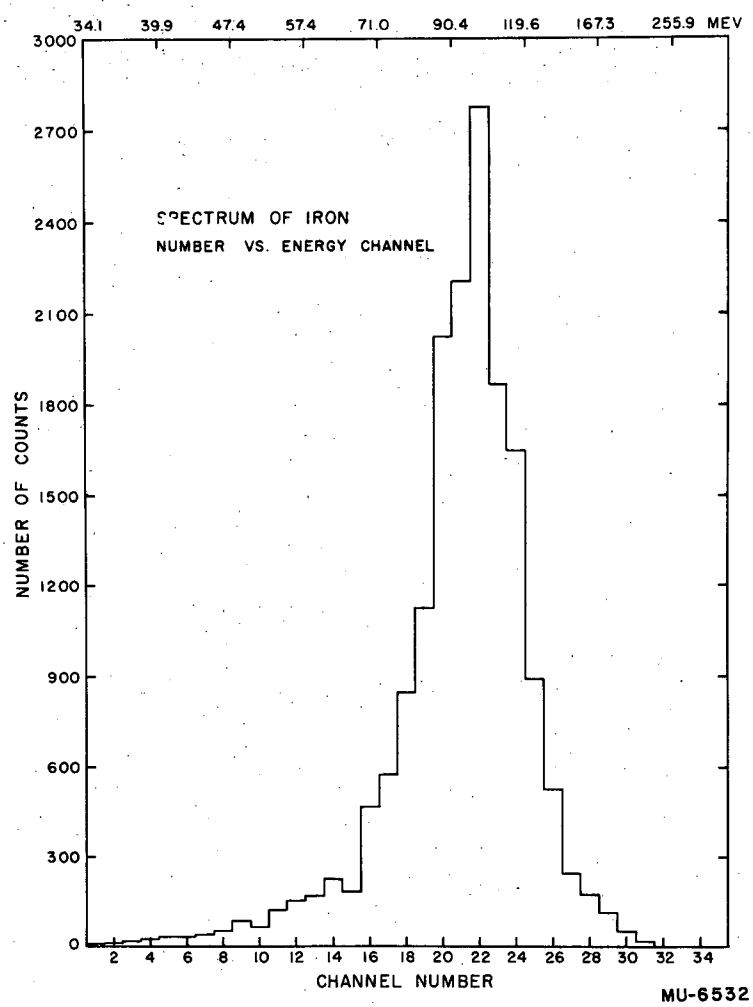

Fig. 14 - Spectrum of Iron

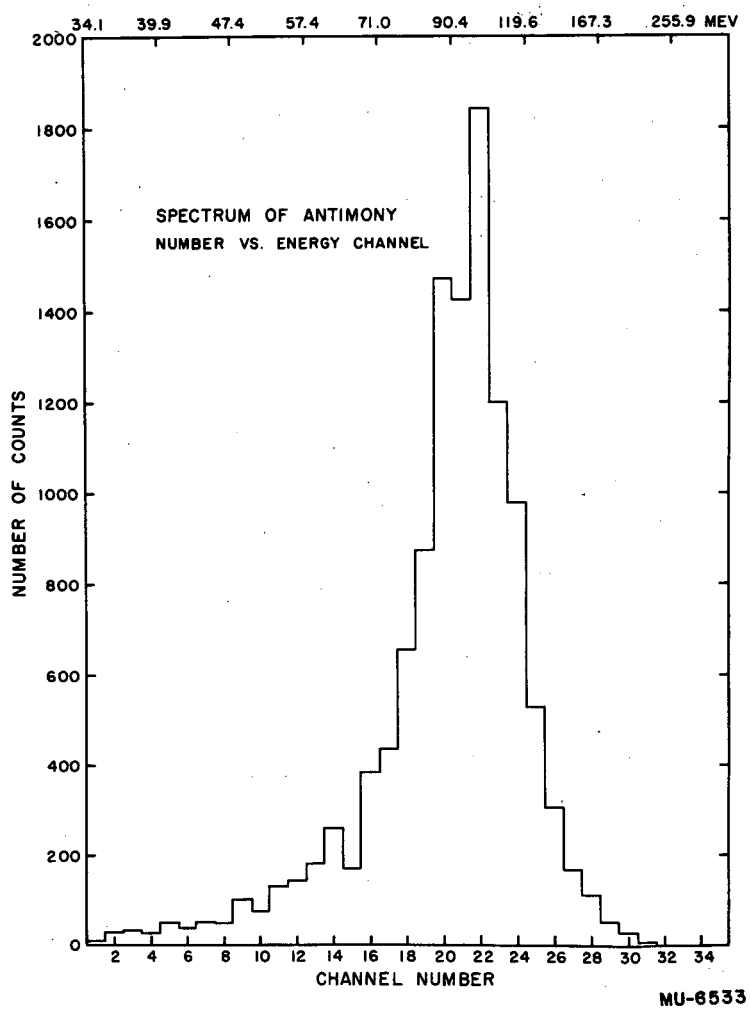

Fig. 15 - Spectrum of Antimony

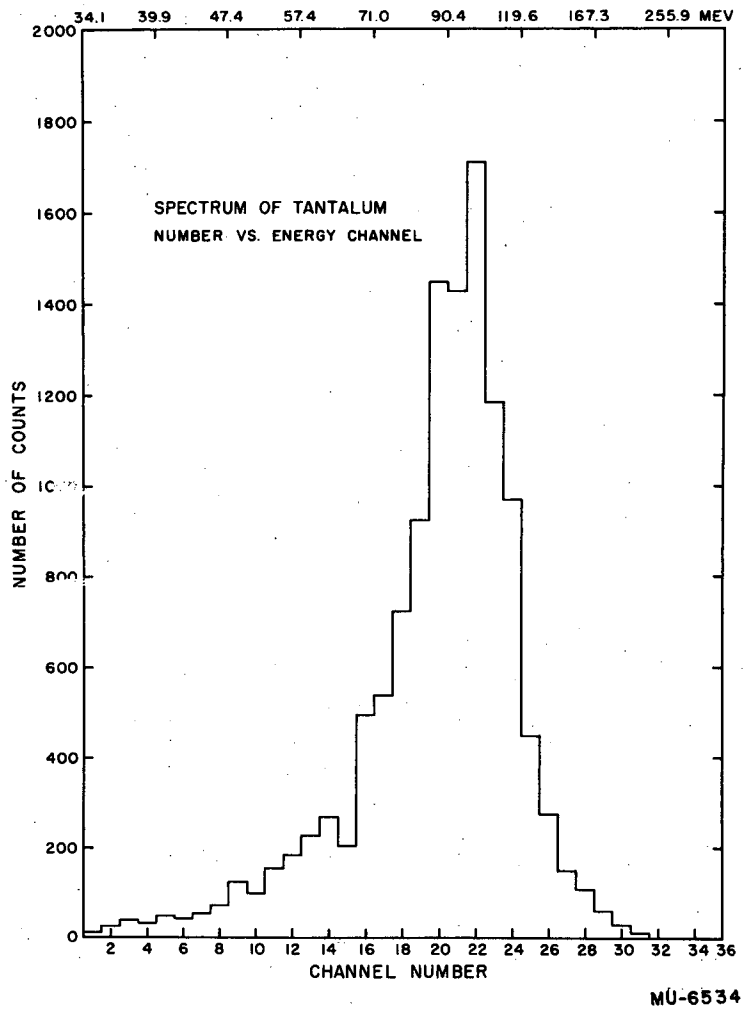

Fig. 16 - Spectrum of Tantalum

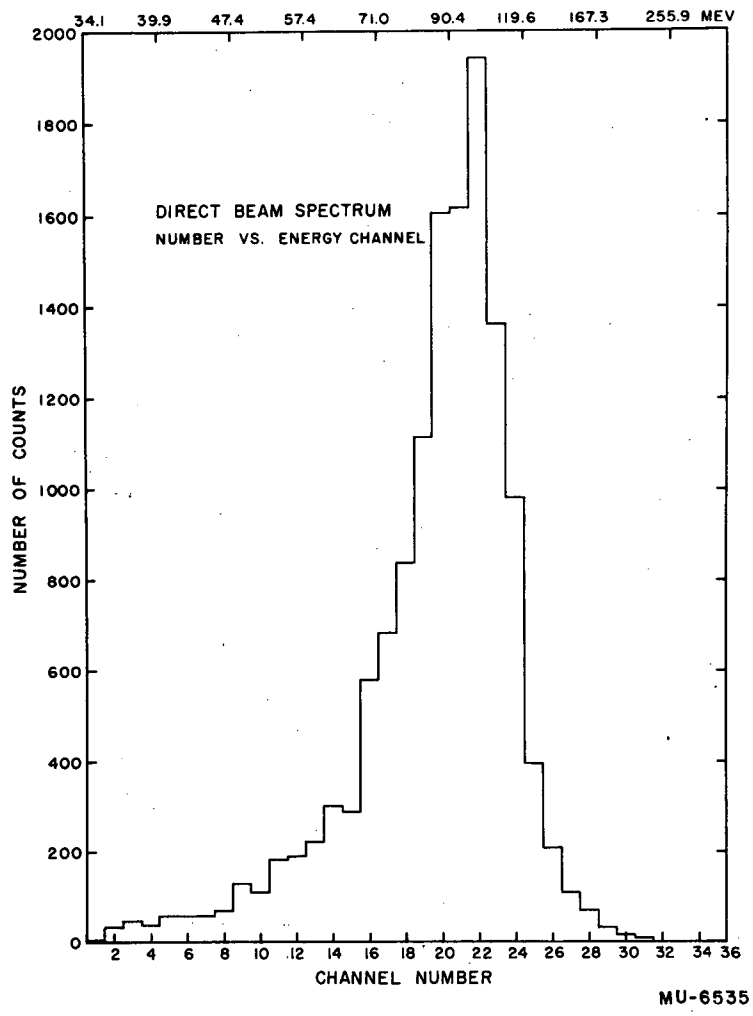

Fig. 17 - Direct Beam Spectrum
Number vs. Energy Channel

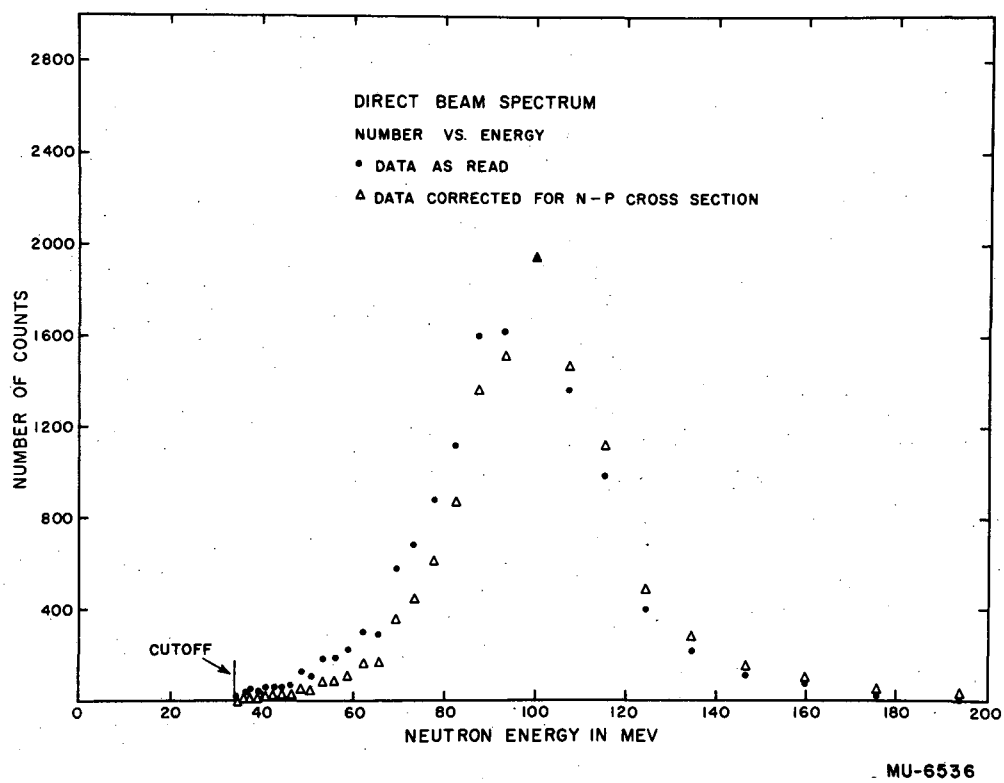

Fig. 18 - Direct Beam Spectrum
Number vs. Energy

TOTAL CROSS SECTIONS

Individual Channels

Total Cross Section in Millibarns

Channel Number	Energy (Mev)	Carbon	Iron	Antimony	Tantalum
1	34.8 ± 0.7		1491 ± 680	1429 ± 956	1712 ± 1220
2	36.1 ± 0.7		2948 ± 287	3269 ± 309	4445 ± 399
3	37.6 ± 0.8		2753 ± 234	3472 ± 273	4350 ± 350
4	39.1 ± 0.8	880 ± 103	2332 ± 199	3519 ± 182	4382 ± 376
5	40.8 ± 0.9	1023 ± 124	2477 ± 171	3242 ± 228	4425 ± 306
6	42.6 ± 0.9	1142 ± 186	2477 ± 171	3600 ± 248	4566 ± 320
7	44.4 ± 1.0	903 ± 89	2324 ± 162	3157 ± 224	4174 ± 244
8	46.4 ± 1.1	748 ± 54	2236 ± 142	3442 ± 218	4039 ± 260
9	48.6 ± 1.2	858 ± 52	2361 ± 108	3382 ± 156	4202 ± 194
10	50.9 ± 1.2	828 ± 53	2472 ± 123	3528 ± 174	4255 ± 214
11	53.4 ± 1.3	717 ± 31	2349 ± 91	3451 ± 134	4327 ± 168
12	56.0 ± 1.4	717 ± 30	2189 ± 85	3389 ± 130	4117 ± 160
13	58.9 ± 1.5	724 ± 28	2233 ± 79	3316 ± 118	4033 ± 145
14	62.1 ± 1.7	708 ± 23	2242 ± 69	3241 ± 100	4225 ± 130
15	65.4 ± 1.8	704 ± 24	2265 ± 71	3687 ± 114	4603 ± 107
16	69.1 ± 2.0	680 ± 16	2243 ± 49	3560 ± 78	4212 ± 94
17	73.1 ± 2.1	629 ± 13	2173 ± 45	3600 ± 73	4430 ± 88
18	77.5 ± 2.3	593 ± 11	2017 ± 38	3360 ± 62	4293 ± 79
19	82.3 ± 2.6	585 ± 9	2022 ± 33	3356 ± 53	4350 ± 69
20	87.6 ± 2.8	520 ± 7	1851 ± 26	3170 ± 43	4218 ± 56
21	93.4 ± 3.2	509 ± 7	1789 ± 26	3219 ± 43	4247 ± 56
22	100.0 ± 3.6	475 ± 6	1753 ± 23	3131 ± 38	4256 ± 52
23	107.2 ± 3.9	472 ± 7	1790 ± 28	3221 ± 47	4285 ± 62
24	115.3 ± 4.4	439 ± 8	1629 ± 31	3077 ± 53	4082 ± 70
25	124.4 ± 5.0	389 ± 11	1398 ± 47	2725 ± 78	3850 ± 107
26	134.8 ± 5.7	365 ± 15	1319 ± 64	2636 ± 106	3634 ± 142
27	146.5 ± 6.4	340 ± 20	1395 ± 91	2579 ± 145	3605 ± 196
28	160.0 ± 7.5	379 ± 26	1331 ± 110	2530 ± 180	3434 ± 243
29	175.7 ± 8.6	269 ± 38	1027 ± 144	2459 ± 268	3081 ± 347
30	194.0 ± 10.2	337 ± 53	1241 ± 229	2495 ± 376	3302 ± 495
Normalization to σ_{carbon} = 475 ± 10 mb at 100 Mev					
$\sigma_{norm} \pm \Delta\sigma_{norm}$ =		475 ± 10	1753 ± 52	3131 ± 80	4256 ± 106

TABLE II

TOTAL CROSS SECTIONS

Grouped Channels

Total Cross Sections in Millibarns

Channel Groupings	Energy (Mev)	Carbon	Iron	Antimony	Tantalum
1,2,3,4,5	38.6 ± 3.0		2503 ± 98	[illegible]	[illegible]
2,3,4,5	38.6 ± 2.5			3275 ± 135	4306 ± 178
2,3,4,5,6	39.6 ± 3.1	1060 ± 71			
6,7,8	44.5 ± 2.3		2287 ± 90	3299 ± 132	4106 ± 166
7,8,9,10,11	49.5 ± 4.4	771 ± 21			
9,10,11	51.1 ± 2.8		2338 ± 61	3361 ± 88	4137 ± 111
12,13,14	59.3 ± 3.6	704 ± 16	2179 ± 44	3308 ± 66	4015 ± 83
15,16,17	70.1 ± 4.7	651 ± 9	2157 ± 29	3510 ± 48	4278 ± 59
18,19	79.9 ± 4.0	577 ± 7	1978 ± 25	3296 ± 40	4205 ± 52
20,21	90.4 ± 4.9	503 ± 5	1777 ± 19	3105 ± 30	4105 ± 39
22,23	102.8 ± 5.9	462 ± 4	1713 ± 18	3080 ± 30	4147 ± 39
24,25	118.5 ± 7.4	412 ± 6	1504 ± 26	2871 ± 44	3886 ± 58
26,27	138.4 ± 9.4	345 ± 12	1300 ± 52	2529 ± 86	3507 ± 103
28,29	165.2 ± 12.6	327 ± 21	1181 ± 90	2416 ± 149	
28,29,30	166.2 ± 16.8				3196 ± 269
Normalization to σ_{carbon} = 462 ± 6 mb at 102.8 Mev					
$\sigma_{norm} \pm \Delta\sigma_{norm}$ =		462 ± 6	1713 ± 33	3080 ± 52	4147 ± 69

TABLE III

DISCUSSION OF RESULTS

The results for tantalum, antimony, iron, and carbon are given in Tables II and III and Figs. 8 to 12. The general features of the cross-section curves seem to be similar to the results for different elements measured elsewhere. Tantalum seems to exhibit a dip in cross section after which the cross section rises to a maximum value through about 60 to 70 Mev. Antimony may also exhibit a dip in a similar energy region, although the statistics do not preclude a relatively flat curve through this region. The cross section for iron rises in going from high to low energies, exhibiting a rather flat region from 50 to 70 Mev.

Curves for the total cross section for carbon are perhaps the most surprising. In going from high to low energies the curve rises slowly at first, in agreement with the results of other observers. In the region of 50 to 70 Mev the grouped data show a considerably lower cross section than that measured by the Harwell results.[9] The individual channel data would even hint at a relatively flat region from 50 to 70 Mev.

The data for higher Z or A elements also indicated a relatively deep dip in this same energy region.[10] The position of the dip did not change appreciably in going from Z = 92 to Z = 82, although the depth of the dip may have decreased somewhat in going to lower Z elements.

A calculation based on the optical model, or rather on a straightforward quantum mechanical calculation assuming a complex potential and reasonable nuclear radii, has been carried on concurrently with the work described above by Dr. Sidney Fernbach of the Radiation

Laboratory of the University of California. The calculation has been attempted on an exact basis using the Univac electronic computing machines of the Radiation Laboratory. The results, to date, do not appear extremely favorable in explaining the rather rapid change in cross section in the region of the dip.[17] The model does seem to be able to predict a maximum at roughly the right energies,[17,18] but the detailed behaviour of the cross-section curve shows much more gentle variations than the experimental data reveal. In order to reproduce these dips in detail, rather violent changes in the potential seem to be indicated.

If, for the moment, it is assumed that the data actually do agree with the following general behaviour, that is, that the dip occurs at the same energy for all elements measured, but that the depth of the dip decreases as we go to lower-A elements, then we may infer the following conclusions. First, the effect does not depend exclusively on the size of the nucleus but is common to all nuclei, with the possible exception of very low-Z elements. Secondly, this effect does not preclude optical effects and may be a superposition of a gross optical effect upon a detailed effect. Thirdly, the wave length of the neutron in this energy region, i.e., from 50 to 70 Mev or $\lambda\!\!\!^{-} \sim 0.6 \times 10^{-13}$, must be a fundamental length associated with all nuclei.

It must be emphasized, however, that the data, especially for the lower Z elements, are still inconclusive in this regard. Future experiments are planned to investigate this point in greater detail.

In summary, the data of this experiment show an extension in the behaviour of the total neutron cross section curves for Z = 92, 83, and 82, to Z = 73 tantalum. The similar behaviour of Z = 51, antimony is

hinted, but not definitely established. Iron, $Z = 26$, and carbon, $Z = 6$ may also exhibit such behaviour, but here the evidence is even less conclusive.

ACKNOWLEDGEMENTS

The author wishes to extend his thanks for the advice and encouragement of many members of the staff of the Radiation Laboratory; especially to Drs. H. F. York, for his original suggestion of the time of flight technique, L. W. Alvarez, under whose guidance the work has proceeded, B. J. Moyer, for interest and discussions; Messrs. Vern Ogren and Donald Paxson for their invaluable aid with the electronics; Messrs. Robert Silver and John Leahy for help in the cyclotron runs; and to the entire cyclotron crew for cooperation. To Dr. W. I. Linlor, co-worker in all phases of this experiment, goes an especial vote of thanks for his sincere cooperation and understanding. Finally, to my wife I extend my heartfelt thanks for patience, encouragement and confidence.

This work was performed under the auspices of the Atomic Energy Commission.

REFERENCES

1. Miller, Adair, Bockelman, and Darnden, Phys. Rev. 88, 83, (1952)
   H. H. Barschall, Phys. Rev. 86, 431, (1952)
2. H. Feshbach, C. E. Porter, and V. F. Weisskopf, Phys. Rev. 90, 166, (1953)
3. R. Serber, Phys. Rev. 72, 1114, (1947)
4. S. Fernbach, R. Serber, and T. B. Taylor, Phys. Rev. 75, 1352, (1949)
   G. Memmert, Zeit f. Phys. 134, 42, (1952)
5. L. J. Cook. E. M. McMillan, J. M. Peterson, and D. C. Sewell, Phys. Rev. 75, 7, (1949)
6. R. H. Hildebrand and C. E. Leith, Phys. Rev. 80, 842, (1950)
7. J. DeJuren and N. Knable, Phys. Rev. 77, 606, (1950)
   J. DeJuren and B. J. Moyer, Phys. Rev. 81, 919, (1951)
8. A. E. Taylor and E. Wood, Phys. Rev. 87, 907, (1952)
9. A. E. Taylor and E. Wood, Phil. Mag. 44, 95, (1953)
10. W. I. Linlor, UCRL 2303
    W. I. Linlor and B. Ragent, UCRL 2294
11. W. I. Linlor and B. Ragent, Phys. Rev. 91, 440, (1953) Abs. D2
12. B. Ragent and W. I. Linlor, Phys. Rev. 91, 440, (1953) Abs. D3
13. R. Serber, Phys. Rev. 72, 1008, (1947)
14. Mott, Guernsey, and Nelson, Phys. Rev. 88, 9, (1952)
15. J. DeJuren, UCRL 736
16. E. M. McMillan and D. Sewell, MDDC 1558
17. S. Fernbach, Private Communication
18. J. D. Lawson, Phil. Mag. 44, 102, (1953)
19. R. H. Hildebrand, D. A. Hicks, and W. H. Harker, UCRL 1305